Redox sensing by SENP1 augments insulin secretion early after high-fat feeding in mice

Haopeng Lin[1, 2]†, Kunimasa Suzuki[1, 2]†, Nancy Smith[1, 2], Xi Li[3], Lisa Nalbach[4], Sonia Fuentes[3], Aliya F Spigelman[1, 2], Xiaoqing Dai[1, 2], Austin Bautista[1, 2], Mourad Ferdaoussi[6], Saloni Aggarwal[7], Andrew R Pepper[7], Leticia P Roma[5], Emmanuel Ampofo[4], Wen-hong Li[3], Patrick E MacDonald[1, 2] *

1. Department of Pharmacology, University of Alberta, Edmonton, AB T6G 2E1, Canada.
2. Alberta Diabetes Institute, University of Alberta, Edmonton, T6G 2E1, Canada.
3. Departments of Cell Biology and Biochemistry, University of Texas Southwestern Medical Center, 6000 Harry Hines Blvd., Dallas, TX 75390-9039, USA.
4. Institute for Clinical & Experimental Surgery, Saarland University, Homburg/Saar, Germany.
5. Biophysics Department, Center for Human and Molecular Biology, Saarland University, Homburg/Saar, Germany.
6. Department of Pediatrics, University of Alberta, Edmonton, T6G 2E1, Canada.
7. Department of Surgery, University of Alberta, Edmonton, T6G 2E1, Canada.

†. These authors contributed to this study equally.

*Correspondence to:
Patrick MacDonald
Alberta Diabetes Institute
LKS Rm. 6-126
University of Alberta
Edmonton, AB, Canada
T6G 2E1
pmacdonald@ualberta.ca
twitter. @bcellorg
web. www.bcell.org

9,789 words (including references, excluding figure legends)

6 figures; 5 supplementary figures; 3 supplementary tables

Abstract

Pancreatic β-cells respond to metabolic stress by upregulating insulin secretion, however underlying mechanisms remain unclear. In β-cells from overweight humans without diabetes, and mice fed high-fat diet (HFD) for as little as 2 days, insulin exocytosis and secretion are enhanced without increased Ca^{2+} influx. β-cell RNA-seq suggests altered metabolic pathways linked to cytosolic redox following HFD. The increased β-cell exocytosis upon HFD is dependent on a shift towards a reduced intracellular redox state, and increased expression of sentrin-specific protease-1 (*Senp1*). Mechanistically, allosteric binding of Zn^{2+} at a site that includes C535 suppresses basal SENP1 activity and unrestrained β-cell exocytosis and increases SENP1 sensitivity to activation by redox signals. Mice with pancreas- or β-cell SENP1 deletion fail to up-regulate exocytosis after 2-day HFD and become rapidly glucose intolerant. This highlights a key role for Zn^{2+}-dependent redox signaling via SENP1 in β-cell functional responses to metabolic stress. (Words: 145)

Teaser

Early after high fat feeding in mice, a cytosolic reducing signal acting via SENP1 increases the capacity of β-cells to secrete insulin.

MAIN TEXT

Introduction

Type 2 diabetes (T2D) occurs when insulin secretion from pancreatic β-cells fails to meet peripheral demand, which is increased with insulin resistance often coincident with obesity (*1*). While obesity and insulin resistance are major risk factors for T2D, most obese individuals maintain normoglycemia as insulin secretion is increased adequately through the up-regulation of β-cell function and mass (*2–4*), although the relative contribution of each remains unclear (*1*). Up-regulation of β-cell insulin secretory capacity precedes increases in islet mass in mice on a high-fat diet (HFD), and at early time points β-cell functional changes likely outweigh structural changes in increased insulin responses (*5*, *6*). Loss of β-cell function up-regulation may contribute to early progression and deterioration to T2D even with intact β-cell mass (*7*).

Upon short-term starvation, insulin secretion is attenuated with a shift from glucose metabolism to fatty acid oxidation (*8*). On the other hand, overnutrition leads to a compensatory increase of insulin secretion with adaptations in β-cell stimulus-secretion coupling. These include enhanced intracellular Ca^{2+} ($[Ca^{2+}]_i$) responses and up-regulation of metabolic coupling factors that potentiate Ca^{2+} efficacy and amplify insulin secretion (*9–11*). Of note, the latter seem particularly important in adaptation of insulin secretory capacity to metabolic stress. In a longitudinal study measuring parallel β-cell insulin secretion and $[Ca^{2+}]_i$ responses, the efficacy of Ca^{2+}-induced insulin secretion was enhanced via Epac signaling in the early stages of prediabetes (*5*). This may be also accompanied by up-regulation of reducing equivalents (*12–14*) and the exocytotic machinery *per se* in prediabetes (*15*), subsequently followed by a reduced expression in T2D (*16*).

SUMOylation is the posttranslational conjugation of small ubiquitin-like modifier (SUMO) peptides to target proteins, which can be reversed by the sentrin-specific proteases (SENPs) such as SENP1. The activity of SENP1 is subject to redox regulation (*17*). Glucose stimulation of β-cells increases cytosolic reducing signals (*18*, *19*) and enhances insulin secretion in part via SENP1, which modifies exocytotic proteins and facilitates insulin granule priming without significantly affecting Ca^{2+} entry (*20*, *21*). In a chronic overnutrition model glucose-stimulated insulin secretion (GSIS) is impaired, in part due to partial inactivation of SENP1 by oxidative stress (*22*, *23*). In contrast, it remains unknown whether, at an early compensatory or prediabetic stage, altered redox state and SENP1 activity affect β-cell functional compensation and glucose homeostasis.

To this aim, we assessed the role for redox signaling in up-regulation of β-cell exocytosis responses that we find to occur rapidly upon high fat feeding in mice. We also define the molecular

mechanisms by which redox signals impact SENP1 activity, identifying an important interaction between Zn^{2+} binding and redox sensing at cysteine 535 (C535) near the enzyme catalytic site. And finally, using islet- and β-cell–specific SENP1 knockout mice we demonstrate the requirement for SENP1 in mediating the short-term β-cell functional responses and maintenance of glucose homeostasis within 2 days of high fat feeding. This work demonstrates that an acute reduction in β-cell redox state enhances insulin exocytosis via SENP1, critically mediated by an interaction between redox and Zn^{2+} binding at C535, and that this is required for the short-term maintenance of glucose homeostasis in mice.

Results

Higher β-cell secretory capacity from overweight humans and short-term HFD-fed mice

Islets from human donors of 21-45 years of age with BMI >25 exhibited significantly elevated glucose-stimulated insulin secretion (GSIS) compared to similarly aged donors with BMI <25. This increased functionality was lost in T2D (BMI > 25) (**Fig. 1A**). Depolarization-induced β-cell exocytosis is amplified by glucose (*20*). Intriguingly, β-cells from the donors with BMI >25 did not show any difference in depolarization-induced exocytosis compared to BMI <25 at 5 or 10 mM glucose. Instead, the exocytotic response was elevated in the donors with BMI>25 at 1 mM glucose, indicative of an increased insulin granule priming or amplifying effect occurring even at low glucose (**Fig. 1B**), a response that was missing in β-cells of donors with T2D. These differences were not as clear in islets and β-cells from older donors (age >45), although islets and β-cells from older donors with T2D still showed lower insulin secretion and exocytosis respectively compared to donors of similar age and BMI without diabetes (**Fig. 1C, D**).

Although we cannot directly replicate the above conditions in mice, we investigated β-cell functional changes that occur early under metabolic stress in male C57BL/6 mice fed either a chow diet (CD) or HFD for 2 days. Mice fed a 2-day HFD maintained normal glucose tolerance in an intraperitoneal glucose tolerance test (IPGTT) (**Fig. 1E**), along with increased plasma insulin (**Fig. 1F**). Islets from 2-day HFD mice showed increased GSIS (**Fig. 1G**), without any effect on insulin content (**Fig. 1H**). Comparatively, after a 4-week HFD, mice were glucose intolerant (**Fig. S1A**) with increased plasma insulin (**Fig. S1B**) and increased insulin content and enhanced *in vitro* islet insulin secretion (**Fig. S1C, D**). In β-cells from 2-day (**Fig. 1I**) and 4-week (**Fig. S1F**) HFD fed mice, exocytotic responses are increased at low glucose, to the same level as in glucose-stimulated cells. This suggests that signals which amplify insulin exocytosis may be up-regulated, even at low

glucose. There were no differences in voltage-activated Ca^{+} charge entry (**Fig. 1J**) and intracellular Ca^{2+} responses (**Fig. 1K**; **Fig. S1G**), consistent with previous demonstrations of 'increased Ca^{2+} efficacy' under short-term HFD (*5*). Indeed, under conditions that 'clamp' intracellular Ca^{2+} responses to assess glucose-dependent amplification of insulin secretion (*24*), islets from 4-week HFD fed mice exhibited enhanced KCl-stimulated insulin secretion only at low glucose (**Fig. S1E**).

Metabolic pathway remodeling favors reductive signals in islets after short-term HFD

To gain insight into the mechanism that may contribute to increased insulin secretory function following short-term HFD (*25*), we performed RNA sequencing on FACS-sorted β-cells from 2-day CD and HFD mice. We found 213 differentially expressed (DE) genes (**Fig. 2A**). Enrichment analysis of DE genes identified pathways (PW) involved in β-cell functional compensation, such as histone methylation (*26*), MAPK signaling, cholesterol biosynthesis, insulin receptor signaling, and ER-associated misfolded protein response (**Fig. 2B**) (*26*, *27*). As the most significantly enriched pathway, histone methylation can control the transcriptomic efficiency. To examine how those genes involved in histone methylation can interact or overlap with genes in other enriched pathways, all DE genes were submitted to the STRING database (*28*) for protein-protein interaction (**Fig. 2B**). Histone methylation related genes can interact or overlap with genes in other pathways, such as MAPK signaling, consistent with the ability of methylation to adapt insulin secretion through MAPK and regulation of glucose metabolism (*26*).

Gene set enrichment analysis (GSEA) showed that up-regulated genes were enriched for oxidative phosphorylation and glycolysis pathways (**Fig. 2C**). For example, *Cdk1* (the most upregulated gene) and *Ccnb2* increase oxygen consumption rate, citrate cycling and NADPH production in β-cells (**Fig. 2A, D**) (*29*), suggesting that upon 2-day HFD β-cells could favor production of NADPH in the cytosol (**Fig. 2D**). Interestingly, the cholesterol biosynthesis pathway (*Fdft1*, *Hsd17b7*, *Msmo1*, *Fdps*, *Hmgcs1*) was the second most significantly down-regulated (**Fig. 2C, D**). It is widely accepted that cholesterol biosynthesis is a heavily NADPH-consuming anabolic process (*30*), and its inhibition may enhance insulin secretion by increasing NADPH (*31*). Therefore, the downregulation of cholesterol biosynthesis genes could spare cytosolic NADPH for the amplification of insulin release (**Fig. 2D**). Collectively, these results indicate that HFD remodels the metabolic preference in a way that may reduce the cytosolic redox state.

Increased β-cell exocytosis after 2-day HFD requires a reducing signal

Consistent with upregulated transcripts involved in oxidative phosphorylation, islets from 2-day HFD-fed mice consumed higher oxygen at 2.8 mM glucose compared with chow-fed mice (**Fig. 3A**), similar to reports from a 3-month HFD model (*32*). However, we confirmed in islets of mice expressing the cytosolic redox sensor Cyto-roGFP2-Orp1(*33*) that the cytosol in β-cells from 2-day HFD-fed mice was more reduced compared to control mice fed CD (**Fig. 3B**). A reduced redox state appears responsible for enhanced β-cell exocytosis at low glucose after HFD, since this was recapitulated in β-cells of CD-fed mice upon direct intracellular infusion of reduced glutathione (GSH), which could not increase exocytosis further in β-cells of HFD-fed mice (**Fig. 3C**). Conversely, the elevated exocytosis in β-cells after HFD was reversed by direct intracellular application of H_2O_2 (**Fig. 3D**). Previously we showed that the SUMO-protease SENP1 couples redox state to insulin exocytosis (**Fig. 3E**) (*20*). Our transcriptomic analysis indicated an upregulation of *Senp1* in β-cells after 2-day HFD (**Fig. 3F**), which we confirmed by qPCR (**Fig. 3G**). Direct intracellular infusion of active SENP1 catalytic protein increases exocytosis in β-cells from CD-fed mice but, like GSH, cannot increase exocytosis further in the β-cells of HFD-fed mice (**Fig. 3H**). These data suggest that short-term HFD leads to a reduced cytosolic redox state that augments β-cell exocytosis, possibly via SENP1 activation.

Redox regulation of exocytosis requires SENP1 C535

SENP1, a cysteine protease, is subject to redox regulation via a thiol group on the catalytic cysteine C603 or other cysteines (*17*). Required for deSUMOylation, C603 is the most conserved cysteine across SENP isoforms and species, while C535 is the least conserved near the active site (**Fig. 4A**). Although redox regulation of intra-molecular disulfide bonds may control cysteine protease activity, as in GRX1 and TRX1 (*34*), the key cysteines of the SENP1 catalytic domain appear too distant from the catalytic C603 to facilitate such regulation (*35*) (**Fig. 4B**). We therefore generated a series of recombinant SENP1 catalytic domain proteins with cysteine-to-serine substitutions (C535S, C560S, C603S, C613S, and C608S) and measured SUMO-protease activity *in vitro* (**Fig. S2A, Fig. 4C**). While the C603S mutant completely lost SENP1 activity as expected, the C535S mutant maintained 2-fold higher constitutive activity (**Fig. 4C**) and was relatively resistant to inactivation by H_2O_2 (IC_{50}=2.5 mM) compared to SENP1 wild type (WT) (IC_{50}= 1 mM) (**Fig. 4D**). Infusion of either SENP1 WT or C535S to human β-cells was able to increase exocytotic capacity at low glucose (**Fig. 4E**). However, while co-infusion of H_2O_2 blocked the action of

SENP1 WT, the C535S mutant maintained its functional activity (**Fig. 4E**), suggesting that C535 modulates SENP1 sensitivity to oxidative inactivation.

Zn^{2+} sensitizes redox-inhibition of SENP1

SENP1 activity is important for insulin secretion (*20*, *21*). However, SENP1 appears too insensitive to *in vitro* oxidation to serve this purpose *in vivo*. We noticed initially that Ni^{2+}, leached out from Ni^{2+}-NTA agarose during purification, strongly inhibited SENP1 activity (not shown). However, Ni^{2+} is relatively low within cells (*36*), and therefore unlikely to regulate physiological SENP1 activity. Since Zn^{2+} is abundant in β-cells (*36*) and known to inhibit other cysteine-proteases (*37*), it may be a key factor to suppress SENP1 activity. C603-C535-H533 is a predicted Zn^{2+}-binding site in SENP1 (**Fig. 5A, B**). Indeed, Zn^{2+} and Ni^{2+} inhibited SENP1 activity, while other divalent metals such as Ca^{2+} and Co^{2+} had no effect (**Fig. 5C**). The IC_{50} for SENP1 inhibition by Zn^{2+} is right-shifted by nearly-30-fold from 1.1 μM in the WT to 28 μM in the C535S mutant (**Fig. 5D**), and this inhibition can be readily reversed by chelation with EDTA (**Fig. 5E**). Re-folding of SENP1 with Zn^{2+} increases the sensitivity of SENP1 to inactivation by H_2O_2 from a IC_{50} of 0.90 mM to 0.28 mM (**Fig. 5F**). Importantly, the presence of Zn^{2+} allows robust activation of SENP1 activity by GSH and glutaredoxin-1 (GRX1), while this dynamic regulation is lost in the C535S mutant (**Fig. 5G**). Finally intracellular infusion of Zn^{2+}, a direct regulator of insulin secretion (*38*, *39*), reduces β-cell exocytosis. At 1 mM $ZnCl_2$, this occurs via a direct inhibition of Ca^{+} channels, while at 100 μM $ZnCl_2$, exocytosis is inhibited without effects on the depolarized-induced Ca^{2+} current (**Fig. S2C, D**). In β-cells lacking SENP1 (βSENP1-KO), exocytosis is reduced (*20*), and 100 μM $ZnCl_2$ impaired exocytosis of βSENP-WT mouse β-cells without further decreasing exocytosis of βSENP-KO mouse β-cells (**Fig. 5H**).

βSENP-KO mice become rapidly glucose intolerant following HFD

Compared with wild-type littermates, β-cells of βSENP1-KO mice failed to show an up-regulation of exocytosis at low glucose after either a 2-day (**Fig. 6A**) or 4-week (**Fig. 6B**) HFD. After the 2-day HFD, male βSENP1-KO mice became rapidly intolerant of IP glucose compared with βSENP-WT littermates (**Fig. 6C, D**), with an impaired plasma insulin response (**Fig. 6E**). This was similar to findings in a separate pancreas-specific SENP1 knockout line (pSENP1-KO; **Fig. S3**), but less obvious in female βSENP1-KO mice which are more resistant to the development of insulin resistance upon HFD (*40*) (**Fig. S3, 4**). While male pSENP1-KO mice also became more intolerant of oral glucose after 2-day HFD (**Fig. S3**), in general impaired IP glucose intolerance was

more obvious after 2-day HFD (**Fig. 6C-E, Fig. S4, 5**). After 4-week HFD however, oral glucose intolerance became more prominent in the βSENP1-KO females **(Fig. S4G-J**) and males (**Fig. S5D-G**), although again the females were generally more insensitive, consistent with our recent report at 8 weeks of HFD in both the pSENP1-and βSENP1-KO models (*22*).

Discussion

β-cell compensation and decompensation is a determinant of early T2D progression (*41*), yet the underlying mechanisms remain unknown. Here we demonstrate that a reducing signal acting via SENP1 facilitates a β-cell functional upregulation to maintain glucose tolerance very early after high fat feeding. This action of SENP1 relies on redox sensing via C535 and the catalytic C603, which is tuned by an interaction with Zn^{2+}. Notably, the enhanced depolarization-induced exocytosis was observed at low glucose, suggesting an upregulation of insulin granule priming soon after 2-day HFD. This can be recapitulated by infusion of reducing signals or infusion of active SENP1, which exerts a similar priming effect (*21*). The result is an increase in the pool of readily releasable insulin granules before a glucose-dependent electrical response and elevated intracellular Ca^{2+} which subsequently has a larger pool of granules on which to act. This is consistent with the enhanced efficacy of Ca^{2+} in 1-week HFD-fed mice (*5*) and pre-diabetic *db/db* mice (*15*).

Redox signals are important regulators of insulin secretion and functional compensation (*12*, *20*). We observed a remodeling of metabolic pathways in RNAseq data and increased O_2 consumption at low glucose after 2-day HFD, and down-regulation of the cholesterol biosynthesis suggestive of an increase in cytosolic NADPH (*31*). We and others have shown that NADPH, produced by either the mitochondrial export of reducing equivalents or the pentose phosphate pathway (*42*, *43*), augments Ca^{2+}-triggered insulin exocytosis (*20*, *44*, *45*). Interestingly, the most upregulated transcript after the 2-day HFD was *Cdk1*, which increases mitochondrial respiration and modulates the exocytotic machinery (*29*). Other increased transcripts related to the electron transport chain might be also accelerate glucose metabolism. Even so, this didn't seem to affect the Ca^{2+} response to glucose, possibly because ATP was consumed by an increased priming of insulin granules (*46*). Instead, it seems to produce a reduced cytosolic redox, as demonstrated in the Cyto-roGFP2-Orp1 transgenic mice. One caveat is that this redox-sensor reports the steady state balance between oxidizing and reducing signals (*19*, *47*). The reduced redox could result from either decreased H_2O_2 production or increased reducing equivalents shortly after HFD. A recent study found that adaptive glucose metabolism can enhance *de novo* GSH biosynthesis independent of NADPH generation (*48*). Therefore, increased *de novo* GSH biosynthesis could also contribute to

an adaptive increase in insulin secretion. Nonetheless, the reduced cytosolic redox state appears critical for the increased β-cell exocytosis seen after 2-day HFD since it could be reversed by oxidation and replicated by GSH or NADPH as we have shown previously (*20*).

Compared to other SENP isoforms, SENP1 is a redox-sensitive protease with an unique interaction between a free thiol on the catalytic cysteine (C603) and other cysteines (*17*). C613 is reported to be a 'positive' redox sensor by forming an intermolecular disulfide bond with the C603 and protect SENP1 from irreversible oxidation (*17*). We find however that mutation of C613 had little effect on SENP1 activity under the current conditions, but rather that C535 appears to restrain SUMO-protease activity of the SENP1 catalytic core domain. The C535S mutant had 2-fold higher activity was resistant to inactivation by H_2O_2, indicating that C535 is a 'negative' redox sensor with a distinct redox-sensing mechanism. Indeed, the atomic distance between thiols of C535 and C603 prevents formation of an intramolecular disulfide bond, consistent with the absence of disulfide bonds in available SENP1 crystal structures (*35*). We also find that C535 does not control enzyme activity via the formation of intermolecular SENP1 dimers (not shown). Thus, it seems most likely that SENP1 redox-sensing via C535 occurs via a proton transfer pathway, and deprotonation of the thiol group on C603 to activate SENP1. Specifically, proton transfers from the thiol group of C603 to the carboxyl group of D550 via H533 results in the conversion of a thiol on C603 to an active thiolate in SENP1 (*49*). C535 may donate a proton to either H533 or D550, like C603 does, to competitively restrain proton transfer from C603, leading to inhibition of SENP1, under oxidizing conditions (**Fig. S2E**).

The biological relevance of SENP1 in β-cell is coupling reducing power to enhancing glucose-stimulated insulin secretion (*20*, *21*, *50*, *51*). Interestingly, we find that Zn^{2+} allosterically inhibits SENP1 in a manner that is also dependent upon C535. Mechanistically, the predicted Zn^{2+}-binding site includes C603, H533 and C535, which is one of the most ubiquitous Zn^{2+} binding motifs (*52*) and a coordinate bond between Zn^{2+} and these residues likely further restricts proton transfer thus inhibiting SENP1. Indeed, thiol-binding Zn^{2+} readily dissociates in the presence of oxidant, leaving a highly reactive thiolate for oxidant (*53*). Therefore, interaction between C535 and Zn^{2+} sensitizes SENP1 to oxidation and allows robust reactivation by reducing signals. Zn^{2+} inhibits exocytosis via SENP1 with a calculated free Zn^{2+} at ~0.08 μM. However, cytosolic free Zn^{2+} levels are not perturbed by glucose stimulation (*54*) or the short-term HFD (not shown). Rather, the binding of Zn^{2+} to SENP1 is likely important in sensitizing SENP1 to redox regulation and control of β-cell function. As a negative regulator, C535 prevents the hyperactivity of SENP1, which might otherwise abolish the redox regulation of SENP1. Zn^{2+} binding of SENP1 may occur

at the time of protein folding in the ER, or via direct interaction with Zn^{2+}-binding/buffering proteins such as metallothionein 1 (MT1) (~10 μM in the pancreatic islets) which have been shown to control islet Zn^{2+} fluctuations (*55*) and inhibit glucose-stimulated insulin secretion (*56*).

Knockout of islet and β-cell SENP1, in two separate Cre-driver models, led to IP glucose intolerance after 2-day HFD and this was associated with a loss of insulin response in the more specific βSENP1-KO. However, oral glucose tolerance was not different following 2-day HFD in most cases. This contrasts with 4-week HFD, where the SENP1-KO showed selectively impaired oral, not IP, glucose tolerance. This discrepancy lies at the differences of adaptive functional changes at different stages of high fat feeding (*57*). In the long term HFD, oxidative stress leads to SENP1 inactivation, decompensated GSIS and comparable impairment of IP glucose tolerance in both SENP1-WT and SENP1-KO mice (*22*). However, the incretin response is paramount in preventing oral glucose intolerance after long term HFD (*22*, *58*), where incretin release (notably glucose-dependent insulinotropic polypeptide - GIP) from the gut (*22*) and β-cell incretin receptors (*57*) are upregulated. β-cell SENP1 is required for mediating these compensational changes to maintain incretin-stimulated insulin secretion and oral glucose tolerance (*22*, *59*). During the 2-day HFD, functional compensation in the form of enhanced glucose-stimulated insulin secretion requires upregulation of redox signaling via SENP1 for maintaining IP glucose tolerance. In addition, GLP-1 signaling confers glucose competence on β-cell through local GLP-1 or glucagon (*60–62*), such that ablation of SENP1 might impair IP glucose tolerance via reduced functional up-regulation. However, the β-cell GLP-1 receptor is not necessary for oral glucose tolerance under normal conditions (*60*), similar to the role of SENP1 for oral glucose tolerance under the same conditions (*22*) or after 2-day HFD, under which circulating incretins remained low (not shown). Additionally, the extra-islet action of GLP-1 could mask the effect of β-cell SENP1, such that OGTT is similar in βSENP1-KO and -WT mice (*60*). Finally, the less cell-type-selective pSENP1-KO mice, which have impaired GIP-stimulated glucagon secretion (*22*), did show impaired oral glucose tolerance after 2-day HFD, indicating the importance of α-to-β cell communication under this condition and as previously reported (*58*).

Thus, we show that insulin secretion is upregulated from human islets from donors with increased BMI, at early/mid-age, and from mouse islets shortly after HFD. This is not due to an increased Ca^{2+} response in β-cells, but to an increase in the availability of releasable insulin granules that occurs at low glucose (i.e. prior to glucose-stimulation). This requires a reducing signal, mediated by the SUMO-protease SENP1 via a mechanism involving a Zn^{2+}-dependent redox control of enzyme activity by C535 near the enzyme catalytic site. In mice this enhanced

insulin secretory capacity acts to maintain glucose tolerance in the face of a short-term metabolic challenge imposed by high fat feeding.

Materials and Methods

Islet isolation and cell culture. Human islets were isolated at the Alberta Diabetes Institute IsletCore (www.isletcore.ca) and cultured overnight in DMEM (11965, Gibco) supplemented with L-glutamine, 110 mg/l sodium pyruvate, 10 % FBS (12483, Gibco), and 100 U/ml penicillin/streptomycin (15140, Gibco) (*63*). A total of 265 non-diabetic (ND) donors and 34 T2D donors (HbA1c>6.5) (**Table S1**) were examined. Separation of donors by BMI and age was based on clinical diagnostic criteria for overweight, and previous studies by us (*63*) and others (*64*) demonstrating declines in human islet insulin secretion between the ages of 40 and 50. All human islet studies were approved by the Human Research Ethics Board (Pro00013094; Pro00001754) at the University of Alberta and all families of organ donors provided written informed consent.

C57BL/6 mice (Charles River Laboratories) were put on standard chow diet (5L0D*, PicoLab Laboratory Rodent Diet) or 60 % high-fat diet (S3282, Bio-Serv) at 12 weeks of age for 2-days or 4-weeks. Pdx1-Cre mice (B6.FVB-Tg (Pdx1-Cre)6 Tuv/J, Jackson Lab, 014647) on a C57BL/6 background and Ins1-Cre mice on a mixed C57BL/6 and SV129 background (*65*) were crossed with *Senp1*-floxed mice on a C57BL/6 background to generate gut/pancreas specific (Pdx1-Cre^{+};Senp1$^{fl/fl}$ - pSENP1-KO) and β-cell-specific knockouts (Ins1-Cre^{+};Senp1$^{fl/fl}$ - βSENP1-KO) (*20*, *66*). Control littermates Pdx1-Cre^{+};Senp1$^{+/+}$ mice (pSENP1-WT) and Ins1-Cre^{+};Senp1$^{+/+}$ mice (βSENP1-WT) at 12 weeks of age were used for experiments. Genotypes and SENP1 expression were confirmed as previously (*22*). Mouse islets were isolated by collagenase digestion and purified by histopaque density gradient centrifugation before hand-picking (*22*). All mouse islets or single cells were cultured in RPMI-1640 (11875, Gibco) with 11.1 mM glucose, 10 % FBS (12483, Gibco), 100 units/mL penicillin, and 100 mg/mL streptomycin (15140, Gibco). All studies with mice were approved by the Animal Policy and Welfare Committee (AUP00000291) at the University of Alberta.

Insulin secretion. After overnight culture, static insulin secretion was measured as previously (*63*) at the glucose concentrations indicated. Diazoxide and KCl concentration were 100 μM and 30 mM respectively. For dynamic insulin responses 25 islets were pre-perifused for 30 minutes at 2.8 mM glucose followed by 16.7 mM glucose and KCl (30 mM) at a sample collection rate of 100 ul/min

every 2-5 minutes (*22*). Insulin content was extracted with acid/ethanol. The samples were stored at −20°C and assayed by using Insulin Detection Kit (STELLUX® Chemi Rodent Insulin ELISA kit; STELLUX® Chemi Human Insulin ELISA kit, Alpco).

Exocytosis measurements. Human and mouse islets were dispersed to single cells in Ca^{2+}-free buffer and cultured in 5.5 mM glucose DMEM and 11 mM glucose RPMI, respectively as above. After overnight culture, dispersed cells were preincubated at 1 mM (human) or 2.8 mM (mouse) glucose for 1 hour and patched in bath solution containing (in mM): 118 NaCl, 5.6 KCl, 20 TEA, 1.2 $MgCl_2$, 2.6 $CaCl_2$, 5 HEPES at different glucose conditions (1, 2.8, 5, 10 mM) with a pH of 7.4 (adjusted by NaOH) at 32-35ºC. Whole-cell capacitance was recorded with the sine+DC lock-in function of an EPC10 amplifier and PatchMaster software (HEKA Electronics). Exocytotic responses and inward Ca^{2+} currents were measured 1-2 minutes after obtaining the whole-cell configuration in response to ten 500 ms depolarizations to 0 mV from a holding potential of -70 mV. Changes in capacitance and integrated Ca^{2+} charge entry were normalized to cell size (fF/pF and pC/pF, respectively). The intracellular solution contained (in mM): 125 Cs-Glutamate, 10 CsCl, 10 NaCl, 1 $MgCl_2$, 5 HEPES, 0.05 EGTA, 3 MgATP and 0.1 cAMP with pH=7.15 (pH adjusted with CsOH).

In the intracellular infusion experiments, measurements were 2-3 minutes after obtaining the whole-cell configuration. Compounds or recombinant enzymes were added to pipette solution as indicated. For mouse β cells, these were 200 μM H_2O_2 (Sigma), 10 μM reduced glutathione (GSH, Sigma), 4 μg/ml cSENP1 (Enzo Life Technologies) and glutathione-S-transferase (GST) peptide (Enzo Life Technologies) as a control peptide. For human β cells, these were 4 μg/ml GST, wild type SENP1, C535S and C603 mutant recombinant purified proteins (see below) pretreated with or without 200 μM H_2O_2 for 10 minutes. For Zn^{2+} infusion, $ZnCl_2$ was included in the pipette and free Zn^{2+} concentrations were approximated using the web-based MaxChelator program at somapp.ucdmc.ucdavis.edu/pharmacology/bers/maxchelator/webmaxc/webmaxcS.htm. Human β-cells were identified by immunostaining for insulin. Mouse β-cells were identified by size (>4 pF) and a Na^+ channel half-maximal inactivation at around -90 mV (*67*).

Glucose homeostasis. Oral glucose tolerance test (OGTT), intraperitoneal tolerance test (IPGTT) and insulin tolerance test (ITT) were performed as previously described (*22*). For OGTT and IPGTT on chow diet or 2-day HFD, glucose concentration was 1 g/kg dextrose, while on 4-week HFD, it was 0.5 g/kg dextrose. Tail blood was collected at indicated times for insulin (STELLUX® Chemi

Rodent Insulin ELISA kit, Alpco) and glucose measurement. ITT was performed with a concentration of 1 U/kg Humulin R (Eli Lilly).

Intracellular Ca^{2+} imaging. Mouse islet cells were cultured on 35 mm Glass bottom dish with 10 mm micro-well (Cellvis) overnight in 11 mM glucose RPMI media (11875, Thermo Fisher). Cells were pre-incubated with Fura-2AM (1 μM) for 15 min and perifused with KRB solution at indicated glucose level and imaged at 0.5 Hz. Fluorescence signal was excited at 340/380 nm (intensity ratio 20:8) and detected at an emission light of 510 nm using Life Acquisition software (Till Photonics) on an inverted microscope (Zeiss Axioobserver, Carl Zeiss Canada Ltd.) equipped with a rapid-switching light source (Oligochrome; Till Photonics, Grafelfing, Germany). β-cells were marked and identified by immunostaining and fluorescence ratios were calculated using ImageJ (NIH).

Oxygen consumption. Isolated islets incubated overnight were washed 3X with serum-free RPMI media at 2.8 mM glucose. Oxygen consumption rate was measured with Fluorescence Lifetime Micro Oxygen Monitoring System (FOL/C3T175P, Instech Laboratories Inc.). Briefly, around 200 islets were added to the chamber for data collection for 20 minutes. Afterwards, islets were collected and oxygen consumption rate was normalized to DNA content measured using a Quant-iT™ PicoGreen™ dsDNA Assay Kits (Invitrogen).

Recombinant wild-type and mutant SENP1. Human SENP1 catalytic domain cDNA (419-644 residues) was cloned downstream of the His×6 coding sequence, to add a Hisx6 N-terminal tag to SENP1, between Xba-I and BamH-I sites in the pT7JLH plasmid (*68*). Site directed mutagenesis by primer extension was used to make SENP1 mutants, C535S, C560S, C603S, C608S, C613S, C535S/C608S and C603S/C613S. In brief, two sets of overwrapping mutagenesis primers were used to amplify SENP1 catalytic domain using Phusion DNA polymerase. The SENP1 cDNA was cloned between Xba-I and BamH-I sites using Gibson assembly.

For expression, the Rosetta strain of *E. coli* (Novagen) was transformed with each expression vector and grown in 50 ml LB broth containing 100 μg/ml Ampicillin at 37°C with shaking until A600 reached between 0.6 and 0.8. Each SENP1 protein was overexpressed by addition of 1 mM IPTG into the culture. After 2 hours induction, the *E. coli* pellet was harvested by centrifugation at 10,000 × g for 10 minutes. Inclusion bodies of SENP1 proteins were prepared from *E. coli* pellet (*69*). Each protein was solubilized in 6 M guanidine HCl, 20 mM Tris, 0.1 % Tween20, 1 mM 2-mercaptoethanol, pH=8, and captured with a HisPur Nickel-NTA resin column

(1.5 × 3cm). The column was washed with 4 M Guanidine HCl, 20 mM Tris, 0.1 % Tween20, 1 mM 2-mercaptoethanol, pH=8 and then SENP1 protein was eluted with 4 M guanidine HCl, 50 mM Sodium acetate, 0.05 % Tween20, pH=4. The absorbance at 280 nm was measured to estimate protein concentration. SENP1 proteins were stored at -80ºC until *in vitro* refolding.

The purified SENP1 proteins contain Ni^{2+} that was leached out from nickel-NTA resin. For most experiments, Ni^{2+} was removed by protein precipitation in the presence of 20 mM Tris and 5 mM EDTA, pH=8. The concentration of each SENP1 protein was adjusted to 4 mg/ml with 4 M guanidine HCl, 20 mM Tris, 0.1 % Tween20, 1 mM 2-mercaptoethanol, 50 mM EDTA and 0.2 M Tris, pH=8. Ten volumes of water were added to dilute the 4 M guanidine HCl to 0.4 M, which causes the precipitation of SENP1 protein. The precipitated SENP1 protein without nickel was recovered by centrifugation at 8000 × g for 20 minutes.

Refolding of SENP1 protein was carried out *in vitro* by gradual decrease of guanidine HCl concentration with dialysis (*70*). The concentration of SENP1 protein was adjusted to 1 mg/ml with 6 M guanidine HCl, 20 mM Tris, 0.1 % Tween20, 0.2 M Arginine, pH=7.2, and for each refolding 4-5 mg of SENP1 was used. The cysteines of SENP1 proteins were reduced to sulfhydryl with 10 mM DTT for 1 hour at room temperature. The SENP1 proteins were dialyzed against 10 volumes of 0.5 M guanidine HCl, 0.2 M Arginine, 0.1 M Tris, 2 mM Cysteine, 0.2 mM Cystine, 0.05 % Tween20, pH=7.2 for 24 hours, and then against 20 volumes of same solution without guanidine HCl for 24 hours. SENP1 proteins were finally dialyzed against 50 volumes of SENP1 assay buffer, 20 mM Tris, 0.1 M sodium chloride, 0.05 % Tween20, pH=7.2 for 24 hours with changing to fresh buffer twice. The precipitated SENP1 proteins were removed by centrifugation at 8000 × g for 10 minutes. Absorbance at 280 nm of the supernatant were measured to estimate the concentration of SENP1 proteins. For the experiments to study the effect of divalent transient metals on SENP1 activity, 0.1 mM of $CaCl_2$, $CoCl_2$, $NiCl_2$ and $ZnCl_2$ was added in the refolding solution, and then divalent metals were removed by extensive dialysis against SENP1 assay buffer, 20 mM Tris, 0.1 M sodium chloride, 0.05% Tween20, pH=7.2

In vitro SENP1-protease assay. Recombinant Hisx6-SUMO1-mCherry was used as substrate to measure SENP1 activity. The cDNA of full size human SUMO1, including the cleavage site, and mCherry were amplified with PCR using Phusion DNA polymerase and the PCR fragments were cloned into a pT7JLH plasmid at Xba-I site using Gibson assembly to make pT7JLH-SUMO1-mCherry plasmid. Transformed Rosetta strain of *E. coli* was grown in 50 ml LB broth containing 100 μg/ml Ampicillin at 37ºC with shaking until A600 reached between 0.6 and 0.8. Hisx6-

SUMO1-mCherry protein was expressed by slow induction with 0.1 mM IPTG at 20ºC overnight and the *E. coli* pellet was harvested by centrifugation at 10,000 × g for 10 minutes. Pink color of *E. coli* pellet indicated the proper folding of Hisx6-SUMO1-mCherry. The pellet was incubated with 500 μg/ml lysozyme, 1 mM PMSF, 5mM EDTA, 50 mM Tris, 0.2 M sodium chloride, pH=8 for 3 hours at 4ºC, and then sonicated five times in short burst of 30 seconds on ice. The cell lysate was centrifuged at 10,000 × g for 10 minutes at 4ºC, and then the soluble His×6-SUMO1-mCherry in the supernatant was purified with a HisPur Nickel-NTA resin column (1 x 5 cm). The purified Hisx6-SUMO1-mCherry was dialyzed against 10 volumes of 50 mM EDTA, pH=8 for 6 hours and then 50 volumes of SENP1 assay buffer (20 mM Tris, 0.1 M sodium chloride, 0.05 % Tween20, pH=7.2) for 24 hours. The final dialysis buffer was changed to fresh buffer twice. The concentration of His×6-SUMO1-mCherry protein was estimated by the absorbance at 280 nm.

For the assay, 100nM recombinant SENP1 protein is mixed with 2.5 μM of His×6-SUMO1-mCherry, and then was incubated at 37ºC for 2 hours. The mCherry was separated from His×6 tag-SUMO1 upon the cleavage with SENP1. The undigested substrate was captured and removed by the addition of 25 μl of HisPur Nickel-NTA resin suspension (1:1, v/v). After vortexing for 10 seconds, HisPur Nickel-NTA resin was precipitated by centrifugation at 10,000 × g for 30 seconds at 4ºC. Each supernatant was transferred into a 96 well clear bottom black plate and then fluorescent intensity, Ex544 nm/Em615 nm, was measured (**Fig. S2A**).

The coding sequence of human GRX1 was cloned into expression vector, pT7JLH. Recombinant GRX1 was produced in *E. coli*, purified and carried out in vitro refolding as above. The activities of SENP1 mutants were initially compared without being fully activated with DTT, 100nM SENP1 and 2.5 μM Hisx6-SUMO-mCherry were incubated at 37ºC for 2 hours to measure SENP1 mutant activity. Because SENP1 activity changes during storage due oxidation, wild type SENP1 and C535S were fully activated with 10 mM DTT at 4ºC overnight. Amicon Ultra-4 10,000NMWL was used to remove DTT and then replaced the buffer to SENP1 assay buffer, 20 mM Tris, 0.1 M sodium chloride, 0.05 % Tween20, pH=7.2. Final concentration of SENP1 and mutants were estimated by the absorbance at 280 nm. To preserve the activity of SENP1 25 % glycerol (w/w) was added and stored under nitrogen gas at -20ºC.

To determine the IC_{50} for inhibition by H_2O_2 or Zn^{2+}, SENP1 was prepared without $ZnCl_2$ in the refolding. Fully activated wild type SENP1 and C535S (0.1 μM) were incubated with H_2O_2 (0.1-5 mM) for 1 hour at 20ºC. Catalase (20 μg) was added into each tube and then incubated for 30 minutes at 20ºC to remove H_2O_2. For Zn^{2+}, fully activated wild type SENP1 and C535S (0.1 μM) were incubated with $ZnCl_2$ (0.001-10 μM) overnight at 4ºC. *K*i value was calculated at

https://bioinfo-abcc.ncifcrf.gov/IC50_Ki_Converter/index.php (*71*). Free Zn^{2+} level was calculated at https://somapp.ucdmc.ucdavis.edu/pharmacology/bers/maxchelator/.

To determine the effect of Zn^{2+} on H_2O_2 inhibition of SENP1, wild type SENP1 and mutants were refolded with/without 0.1 mM $ZnCl_2$, and then $ZnCl_2$ was removed by dialysis. Fully activated SENP1 and mutant were incubated with various concentration of H_2O_2 for 30 minutes at room temperature. Catalase (20 μg) was added into each tube to remove H_2O_2 and then SENP1 activity was measured. Inactive mutant C603S was used as negative control.

Activation of SENP1 with reducing agents was performed on wild type SENP1 and mutants prepared without $ZnCl_2$ in the refolding buffer, then incubated with 1 μM $ZnCl_2$ for 1 hour to suppress SENP1 activities prior to reactivation by 0.1 mM GSH+10 μg/ml GRX1.

Fluorescence activated cell sorting (FACS) of β-cells and mRNA sequencing. Islet α- and β-cells were identified by ZIGIR vs Ex4-Cy5 through FACS analysis as above (*72*). Total RNA was isolated from sorted β-cells using TRIzol reagent (Invitrogen) according to the manufacturer's protocol and cDNA libraries were prepared using Illumina's TruSeq Stranded mRNA Library Prep kit. The cDNA libraries were validated by TapeStation DNA 1000 High Sensitivity assay (Agilent) and quantified by Qubit dsDNA High Sensitivity assay (Invitrogen). High quality libraries were submitted to the UT Southwestern Next Generation Sequencing Core facility and RNA sequencing was performed using Illumina's NextSeq 500 High Output instrument. Raw reads were processed to transcripts per million (TPM) and differentially expressed (DE) genes were initially determined by using the edgeR package. Genes with P-value<0.1, coefficient of variation (CV) of less than 1, same change of direction (either positive or negative) and specific gene counts range (mean gene counts in at least one experimental group should be higher than 5 RPKM) were considered differentially expressed between CD and HFD. All differentially expressed genes are used for downstream analyses and listed in **Data S1**.

Differentially expressed gene function and enriched pathways were identified with Metascape (http://metascape.org/). KEGG Pathway, GO Biological Processes, Reactome Gene Sets, CORUM, TRRUST and PaGenBase were included in pathway enrichment analysis with a p-value <0.01. Terms with an enrichment factor > 1.5 and a similarity of >0.3 are grouped into a cluster represented by the most significant term (*73*). To examine protein-protein interaction (PPI), STRING database (https://string-db.org/) was used and only PPIs with interaction score higher than 0.70 were retrieved and linked in the circus plot by using R-studio (circlize package) (*28*, *74*). To run an unbiased gene set enrichment analysis (GSEA) (*75*), all Genes with CV of less than 1, same

change of direction and specific gene counts range (at least one experimental group should be higher than 5 RPKM) were submitted and listed in **Data S2**. H.all.v7.4.symbols.gmt[Hallmarks] gene dataset was used as reference data set. Enriched gene sets were considered significant with gene size over 50, false discovery rate less than 0.05, nominal *p*-value less than 0.01.

Redox measurement. Measurements of the intracellular H_2O_2 levels were made using a redox histology approach, as previously described (*33*, *76*, *77*). Briefly, batches of 30 islets were collected and immersed in 50 mM N-ethyl-maleimide (NEM) dissolved in PBS for 20 min for sensor chemical fixation. The NEM was then removed, and islets fixed in 4 % paraformaldehyde for 30 min. After paraformaldehyde removal, the islets were incubated in 100-µL HepatoQuick (Roth, Karlsruhe, Germany) mixed with human citrate plasma (1:2 v/v) and 1 % $CaCl_2$ for 1 h at 37°C. Clots were then incubated in 95 % ethanol at 4 °C overnight and subsequently dehydrated in ethanol prior to paraffin embedding. The paraffin embedded clots were cut in 3 µm thick sections with a semi-automated rotary microtome (Leica Biosystems, Wetzlar, Germany) and placed on silanized glass slides. Images of all the islets in each slide were obtained by the Axio Observer 7 fluorescence microscope (Zeiss, Oberkochen, Germany) with a 20× objective using excitation 405 nm and 488 nm, emission 500-530 nm. The images were analyzed with ImageJ Fiji Software, and the ratio (405/488 nm) was used to compare different groups.

Statistical analysis. Analysis was performed using FitMaster (HEKA Electronik) and GraphPad Prism (v7.0c). All data are shown as the mean ± SEM. Statistical outliers were identified and removed by an unbiased ROUT (robust regression followed by outlier identification) test. Normally distributed data were analyzed by the 2-tailed Student's t test (for two groups), or ANOVA and Bonferroni post-test (for multiple groups). Data that failed normality tests were analyzed by the non-parametric Mann-Whitney test (for two groups), or the Kruskal– Wallis one-way analysis of variance followed by Mann-Whitney post-test (for multiple groups). A p-value less than 0.05 was considered significant. Zn^{2+}Bind (https://zincbind.net/) was used to predict the Zn^{2+}-binding site in SENP1 (2IYC) (*78*).

References

1. C. Chen, C. M. Cohrs, J. Stertmann, R. Bozsak, S. Speier, Human beta cell mass and function in diabetes: Recent advances in knowledge and technologies to understand disease pathogenesis. *Molecular Metabolism*. **6**, 943–957 (2017).

2. M. J. Perley, D. M. Kipnis, Plasma insulin responses to oral and intravenous glucose: studies in normal and diabetic subjects. *J Clin Invest*. **46**, 1954–1962 (1967).

3. K. S. Polonsky, B. D. Given, E. Van Cauter, Twenty-four-hour profiles and pulsatile patterns of insulin secretion in normal and obese subjects. *J Clin Invest*. **81**, 442–448 (1988).

4. S. C. Elbein, K. Wegner, S. E. Kahn, Reduced beta-cell compensation to the insulin resistance associated with obesity in members of Caucasian familial type 2 diabetic kindreds. *Diabetes Care*. **23**, 221–227 (2000).

5. C. Chen, H. Chmelova, C. M. Cohrs, J. A. Chouinard, S. R. Jahn, J. Stertmann, I. Uphues, S. Speier, Alterations in β-cell calcium dynamics and efficacy outweigh islet mass adaptation in compensation of insulin resistance and prediabetes onset. *Diabetes*. **65**, 2676–2685 (2016).

6. R. L. Hull, K. Kodama, K. M. Utzschneider, D. B. Carr, R. L. Prigeon, S. E. Kahn, Dietary-fat-induced obesity in mice results in beta cell hyperplasia but not increased insulin release: evidence for specificity of impaired beta cell adaptation. *Diabetologia*. **48**, 1350–1358 (2005).

7. C. M. Cohrs, J. K. Panzer, D. M. Drotar, S. J. Enos, N. Kipke, C. Chen, R. Bozsak, E. Schöniger, F. Ehehalt, M. Distler, A. Brennand, S. R. Bornstein, J. Weitz, M. Solimena, S. Speier, Dysfunction of persisting β Cells is a key feature of early type 2 diabetes pathogenesis. *Cell Rep*. **31**, 107469 (2020).

8. J. Tamarit-Rodríguez, E. Vara, J. Tamarit, Starvation-induced changes of palmitate metabolism and insulin secretion in isolated rat islets stimulated by glucose. *Biochem J*. **221**, 317–324 (1984).

9. M. Z. Khaldi, Y. Guiot, P. Gilon, J. C. Henquin, J. C. Jonas, Increased glucose sensitivity of both triggering and amplifying pathways of insulin secretion in rat islets cultured for 1 wk in high glucose. *American Journal of Physiology-Endocrinology and Metabolism*. **287**, E207–E217 (2004).

10. M. Wortham, M. Sander, Mechanisms of β-cell functional adaptation to changes in workload. *Diabetes Obes Metab*. **18**, 78–86 (2016).

11. M. Fex, M. D. Nitert, N. Wierup, F. Sundler, C. Ling, H. Mulder, Enhanced mitochondrial metabolism may account for the adaptation to insulin resistance in islets from C57BL/6J mice fed a high-fat diet. *Diabetologia*. **50**, 74–83 (2007).

12. E. Irles, P. Ñeco, M. Lluesma, S. Villar-Pazos, J. C. Santos-Silva, J. F. Vettorazzi, P. Alonso-Magdalena, E. M. Carneiro, A. C. Boschero, Á. Nadal, I. Quesada, Enhanced glucose-induced intracellular signaling promotes insulin hypersecretion: pancreatic beta-cell

functional adaptations in a model of genetic obesity and prediabetes. *Molecular and Cellular Endocrinology*. **404**, 46–55 (2015).

13. A. Gonzalez, B. Merino, L. Marroquí, P. Ñeco, P. Alonso-Magdalena, E. Caballero-Garrido, E. Vieira, S. Soriano, R. Gomis, A. Nadal, I. Quesada, Insulin hypersecretion in islets from diet-induced hyperinsulinemic obese female mice is associated with several functional adaptations in individual β-cells. *Endocrinology*. **154**, 3515–3524 (2013).

14. M. M. R. Valle, M. F. R. Graciano, E. R. Lopes de Oliveira, J. P. G. Camporez, E. H. Akamine, C. R. de O. Carvalho, R. Curi, A. R. Carpinelli, Alterations of NADPH oxidase activity in rat pancreatic islets induced by a high-fat diet. *Pancreas*. **40**, 390–395 (2011).

15. O. H. Do, J. E. Gunton, H. Y. Gaisano, P. Thorn, Changes in beta cell function occur in prediabetes and early disease in the Lepr db mouse model of diabetes. *Diabetologia*. **59**, 1222–1230 (2016).

16. N. R. Gandasi, P. Yin, M. Omar-Hmeadi, E. Ottosson Laakso, P. Vikman, S. Barg, Glucose-dependent granule docking limits insulin secretion and is decreased in human type 2 diabetes. *Cell Metabolism*. **27**, 470-478.e4 (2018).

17. Z. Xu, L. S. M. Lam, L. H. Lam, S. F. Chau, T. B. Ng, S. W. N. Au, Molecular basis of the redox regulation of SUMO proteases: a protective mechanism of intermolecular disulfide linkage against irreversible sulfhydryl oxidation. *FASEB J*. **22**, 127–137 (2008).

18. W. D. Cameron, C. V. Bui, A. Hutchinson, P. Loppnau, S. Gräslund, J. V. Rocheleau, Apollo-NADP+ : a spectrally tunable family of genetically encoded sensors for NADP+. *Nature Methods*. **13**, 352–358 (2016).

19. J.-P. Deglasse, L. P. Roma, D. Pastor-Flores, P. Gilon, T. P. Dick, J.-C. Jonas, Glucose acutely reduces cytosolic and mitochondrial H_2O_2 in rat pancreatic beta cells. *Antioxid Redox Signal*. **30**, 297–313 (2019).

20. M. Ferdaoussi, X. Dai, M. V. Jensen, R. Wang, B. S. Peterson, C. Huang, O. Ilkayeva, N. Smith, N. Miller, C. Hajmrle, A. F. Spigelman, R. C. Wright, G. Plummer, K. Suzuki, J. P. Mackay, M. van de Bunt, A. L. Gloyn, T. E. Ryan, L. D. Norquay, M. J. Brosnan, J. K. Trimmer, T. P. Rolph, R. G. Kibbey, J. E. M. Fox, W. F. Colmers, O. S. Shirihai, P. D. Neufer, E. T. H. Yeh, C. B. Newgard, P. E. MacDonald, Isocitrate-to-SENP1 signaling amplifies insulin secretion and rescues dysfunctional β cells. *J Clin Invest*. **125**, 3847–3860 (2015).

21. X.-Q. Dai, G. Plummer, M. Casimir, Y. Kang, C. Hajmrle, H. Y. Gaisano, J. E. Manning Fox, P. E. MacDonald, SUMOylation regulates insulin exocytosis downstream of secretory granule docking in rodents and humans. *Diabetes*. **60**, 838–847 (2011).

22. H. Lin, N. Smith, A. F. Spigelman, K. Suzuki, M. Ferdaoussi, T. A. Alghamdi, S. L. Lewandowski, Y. Jin, A. Bautista, Y. W. Wang, J. E. Manning Fox, M. J. Merrins, J. Buteau, P. E. MacDonald, β-cell knockout of SENP1 reduces responses to incretins and worsens oral glucose tolerance in high-fat diet-fed mice. *Diabetes*. **70**, 2626–2638 (2021).

23. N. Auberval, S. Dal, W. Bietiger, M. Pinget, N. Jeandidier, E. Maillard-Pedracini, V. Schini-Kerth, S. Sigrist, Metabolic and oxidative stress markers in Wistar rats after 2 months on a high-fat diet. *Diabetology & Metabolic Syndrome*. **6**, 130 (2014).

24. M. Gembal, P. Detimary, P. Gilon, Z. Y. Gao, J. C. Henquin, Mechanisms by which glucose can control insulin release independently from its action on adenosine triphosphate-sensitive K^+ channels in mouse β cells. *J. Clin. Invest.* **91**, 871–880 (1993).

25. A. R. Piñeros, H. Gao, W. Wu, Y. Liu, S. A. Tersey, R. G. Mirmira, Single-cell transcriptional profiling of mouse islets following short-term obesogenic dietary intervention. *Metabolites*. **10**, 513 (2020).

26. M. Wortham, F. Liu, J. Y. Fleischman, M. Wallace, F. Mulas, N. K. Vinckier, A. R. Harrington, B. R. Cross, J. Chiou, N. A. Patel, Y. Sui, U. S. Jhala, O. S. Shirihai, M. O. Huising, K. J. Gaulton, C. M. Metallo, M. Sander, Nutrient regulation of the islet epigenome controls adaptive insulin secretion. *bioRxiv preprint* (2019), doi:10.1101/742403.

27. T. Kang, B. B. Boland, P. Jensen, C. Alarcon, A. Nawrocki, J. S. Grimsby, C. J. Rhodes, M. R. Larsen, Characterization of signaling pathways associated with pancreatic β-cell adaptive flexibility in compensation of obesity-linked diabetes in db/db mice. *Mol Cell Proteomics*. **19**, 971–993 (2020).

28. D. Szklarczyk, A. L. Gable, D. Lyon, A. Junge, S. Wyder, J. Huerta-Cepas, M. Simonovic, N. T. Doncheva, J. H. Morris, P. Bork, L. J. Jensen, C. von Mering, STRING v11: protein–protein association networks with increased coverage, supporting functional discovery in genome-wide experimental datasets. *Nucleic Acids Research*. **47**, D607–D613 (2019).

29. T. Gregg, S. M. Sdao, R. S. Dhillon, J. W. Rensvold, S. L. Lewandowski, D. J. Pagliarini, J. M. Denu, M. J. Merrins, Obesity-dependent CDK1 signaling stimulates mitochondrial respiration at complex I in pancreatic β-cells. *J Biol Chem*. **294**, 4656–4666 (2019).

30. N. M. F. S. A. Cerqueira, E. F. Oliveira, D. S. Gesto, D. Santos-Martins, C. Moreira, H. N. Moorthy, M. J. Ramos, P. A. Fernandes, Cholesterol biosynthesis: a mechanistic overview. *Biochemistry*. **55**, 5483–5506 (2016).

31. M. Hao, W. S. Head, S. C. Gunawardana, A. H. Hasty, D. W. Piston, Direct effect of cholesterol on insulin secretion: a novel mechanism for pancreatic beta-cell dysfunction. *Diabetes*. **56**, 2328–2338 (2007).

32. R. Roat, V. Rao, N. M. Doliba, F. M. Matschinsky, J. W. Tobias, E. Garcia, R. S. Ahima, Y. Imai, Alterations of pancreatic islet structure, metabolism and gene expression in diet-Induced obese C57BL/6J mice. *PLOS ONE*. **9**, e86815 (2014).

33. Y. Fujikawa, L. P. Roma, M. C. Sobotta, A. J. Rose, M. B. Diaz, G. Locatelli, M. O. Breckwoldt, T. Misgeld, M. Kerschensteiner, S. Herzig, K. Müller-Decker, T. P. Dick, Mouse redox histology using genetically encoded probes. *Sci Signal*. **9**, rs1 (2016).

34. T. J. Bechtel, E. Weerapana, From structure to redox: the diverse functional roles of disulfides and implications in disease. *Proteomics*. **17**, 1000–1002 (2017).

35. M. Sun, Y. Wang, Q. Zhang, Y. Xia, W. Ge, D. Guo, Prediction of reversible disulfide based on features from local structural signatures. *BMC Genomics*. **18**, 279 (2017).

36. W. P. Wong, N. B. Allen, M. S. Meyers, E. O. Link, X. Zhang, K. W. MacRenaris, M. El Muayed, Exploring the association between demographics, SLC30A8 genotype, and human islet content of zinc, cadmium, copper, iron, manganese and nickel. *Sci Rep*. **7**, 473 (2017).

37. W. Maret, Inhibitory zinc sites in enzymes. *Biometals*. **26**, 197–204 (2013).

38. T. Ghafghazi, M. L. McDANIEL, P. E. Lacy, Zinc-induced inhibition of insulin secretion from isolated rat islets of Langerhans. **30**, 5 (1981).

39. K. G. Slepchenko, N. A. Daniels, A. Guo, Y. V. Li, Autocrine effect of Zn^{2+} on the glucose-stimulated insulin secretion. *Endocrine*. **50**, 110–122 (2015).

40. U. S. Pettersson, T. B. Waldén, P.-O. Carlsson, L. Jansson, M. Phillipson, Female mice are protected against high-fat diet induced metabolic syndrome and increase the regulatory T cell population in adipose tissue. *PLoS ONE*. **7**, e46057 (2012).

41. C. Weyer, C. Bogardus, D. M. Mott, R. E. Pratley, The natural history of insulin secretory dysfunction and insulin resistance in the pathogenesis of type 2 diabetes mellitus. *J Clin Invest*. **104**, 787–794 (1999).

42. M. Prentki, F. M. Matschinsky, S. R. M. Madiraju, Metabolic signaling in fuel-induced insulin secretion. *Cell Metabolism*. **18**, 162–185 (2013).

43. L. Plecitá-Hlavatá, H. Engstová, B. Holendová, J. Tauber, T. Špaček, L. Petrásková, V. Křen, J. Špačková, K. Gotvaldová, J. Ježek, A. Dlasková, K. Smolková, P. Ježek, Mitochondrial superoxide production decreases on glucose-stimulated insulin secretion in pancreatic β cells due to decreasing mitochondrial matrix NADH/NAD+ ratio. *Antioxidants & Redox Signaling*. **33**, 789–815 (2020).

44. T. M. Reinbothe, R. Ivarsson, D.-Q. Li, O. Niazi, X. Jing, E. Zhang, L. Stenson, U. Bryborn, E. Renström, Glutaredoxin-1 mediates NADPH-dependent stimulation of calcium-dependent insulin secretion. *Molecular Endocrinology*. **23**, 893–900 (2009).

45. R. Ivarsson, R. Quintens, S. Dejonghe, K. Tsukamoto, P. in ’t Veld, E. Renström, F. C. Schuit, Redox control of exocytosis: regulatory role of NADPH, thioredoxin, and glutaredoxin. *Diabetes*. **54**, 2132–2142 (2005).

46. N. Takahashi, T. Kadowaki, Y. Yazaki, G. C. R. Ellis-Davies, Y. Miyashita, H. Kasai, Post-priming actions of ATP on Ca^{2+}-dependent exocytosis in pancreatic beta cells. *PNAS*. **96**, 760–765 (1999).

47. M. Gutscher, M. C. Sobotta, G. H. Wabnitz, S. Ballikaya, A. J. Meyer, Y. Samstag, T. P. Dick, Proximity-based protein thiol oxidation by H2O2-scavenging peroxidases. *Journal of Biological Chemistry*. **284**, 31532–31540 (2009).

48. A. Fu, L. van Rooyen, L. Evans, N. Armstrong, D. Avizonis, T. Kin, G. H. Bird, A. Reddy, E. T. Chouchani, M. Liesa-Roig, L. D. Walensky, A. M. James Shapiro, N. N. Danial,

Glucose metabolism and pyruvate carboxylase enhance glutathione synthesis and restrict oxidative stress in pancreatic islets. *Cell Rep*. **37**, 110037 (2021).

49. T. Shi, Y. Han, W. Li, Y. Zhao, Y. Liu, Z. Huang, S. Lu, J. Zhang, Exploring the desumoylation process of SENP1: a study combined MD simulations with QM/MM calculations on SENP1-SUMO1-RanGAP1. *J Chem Inf Model*. **53**, 2360–2368 (2013).

50. G.-F. Zhang, M. V. Jensen, S. M. Gray, K. El, Y. Wang, D. Lu, T. C. Becker, J. E. Campbell, C. B. Newgard, Reductive TCA cycle metabolism fuels glutamine- and glucose-stimulated insulin secretion. *Cell Metab*. **33**, 804-817.e5 (2021).

51. M. Ferdaoussi, J. Fu, X. Dai, J. E. Manning Fox, K. Suzuki, N. Smith, G. Plummer, P. E. MacDonald, SUMOylation and calcium control syntaxin-1A and secretagogin sequestration by tomosyn to regulate insulin exocytosis in human ß cells. *Sci Rep*. **7**, 248 (2017).

52. J. C. Ebert, R. B. Altman, Robust recognition of zinc binding sites in proteins. *Protein Sci*. **17**, 54–65 (2008).

53. K. Kluska, J. Adamczyk, A. Krężel, Metal binding properties, stability and reactivity of zinc fingers. *Coordination Chemistry Reviews*. **367**, 18–64 (2018).

54. J. L. Vinkenborg, T. J. Nicolson, E. A. Bellomo, M. S. Koay, G. A. Rutter, M. Merkx, Imaging of intracellular free Zn2+ in real time using genetically-encoded FRET sensors. *Nat Methods*. **6**, 737–740 (2009).

55. S. Zimny, F. Gogolin, J. Abel, H. Gleichmann, Metallothionein in isolated pancreatic islets of mice: induction by zinc and streptozotocin, a naturally occurring diabetogen. *Arch Toxicol*. **67**, 61–65 (1993).

56. M. Bensellam, Y.-C. Shi, J. Y. Chan, D. R. Laybutt, H. Chae, M. Abou-Samra, E. G. Pappas, H. E. Thomas, P. Gilon, J.-C. Jonas, Metallothionein 1 negatively regulates glucose-stimulated insulin secretion and is differentially expressed in conditions of beta cell compensation and failure in mice and humans. *Diabetologia*. **62**, 2273–2286 (2019).

57. D. Gupta, T. L. Jetton, K. LaRock, N. Monga, B. Satish, J. Lausier, M. Peshavaria, J. L. Leahy, Temporal characterization of β cell-adaptive and -maladaptive mechanisms during chronic high-fat feeding in C57BL/6NTac mice. *J. Biol. Chem.* **292**, 12449–12459 (2017).

58. K. El, S. M. Gray, M. E. Capozzi, E. R. Knuth, E. Jin, B. Svendsen, A. Clifford, J. L. Brown, S. E. Encisco, B. M. Chazotte, K. W. Sloop, D. J. Nunez, M. J. Merrins, D. A. D'Alessio, J. E. Campbell, GIP mediates the incretin effect and glucose tolerance by dual actions on α cells and β cells. *Science Advances*. **7**, eabf1948 (2021).

59. M. Ferdaoussi, N. Smith, H. Lin, A. Bautista, A. F. Spigelman, J. Lyon, X. Dai, J. E. Manning Fox, P. E. MacDonald, Improved glucose tolerance with DPPIV inhibition requires β-cell SENP1 amplification of glucose-stimulated insulin secretion. *Physiol Rep*. **8**, e14420 (2020).

60. E. P. Smith, Z. An, C. Wagner, A. G. Lewis, E. B. Cohen, B. Li, P. Mahbod, D. Sandoval, D. Perez-Tilve, N. Tamarina, L. H. Philipson, D. A. Stoffers, R. J. Seeley, D. A. D'Alessio,

The role of β cell glucagon-like peptide-1 signaling in glucose regulation and response to diabetes drugs. *Cell Metabolism*. **19**, 1050–1057 (2014).

61. M. E. Capozzi, B. Svendsen, S. E. Encisco, S. L. Lewandowski, M. D. Martin, H. Lin, J. L. Jaffe, R. W. Coch, J. M. Haldeman, P. E. MacDonald, M. J. Merrins, D. A. D'Alessio, J. E. Campbell, β Cell tone is defined by proglucagon peptides through cAMP signaling. *JCI Insight*. **4**, 126742 (2019).

62. M. E. Capozzi, J. B. Wait, J. Koech, A. N. Gordon, R. W. Coch, B. Svendsen, B. Finan, D. A. D'Alessio, J. E. Campbell, Glucagon lowers glycemia when β-cells are active. *JCI Insight*. **5**, 129954 (2019).

63. J. Lyon, J. E. Manning Fox, A. F. Spigelman, R. Kim, N. Smith, D. O'Gorman, T. Kin, A. M. J. Shapiro, R. V. Rajotte, P. E. MacDonald, Research-focused isolation of human islets from donors with and without diabetes at the Alberta Diabetes Institute IsletCore. *Endocrinology*. **157**, 560–569 (2016).

64. M. J. Westacott, N. L. Farnsworth, J. R. St Clair, G. Poffenberger, A. Heintz, N. W. Ludin, N. J. Hart, A. C. Powers, R. K. P. Benninger, Age-dependent decline in the coordinated [Ca^{2+}] and insulin secretory dynamics in human pancreatic islets. *Diabetes*. **66**, 2436–2445 (2017).

65. B. Thorens, D. Tarussio, M. A. Maestro, M. Rovira, E. Heikkilä, J. Ferrer, Ins1(Cre) knock-in mice for beta cell-specific gene recombination. *Diabetologia*. **58**, 558–565 (2015).

66. M. Ferdaoussi, N. Smith, H. Lin, A. Bautista, A. F. Spigelman, J. Lyon, X. Dai, J. E. M. Fox, P. E. MacDonald, Improved glucose tolerance with DPPIV inhibition requires β-cell SENP1 amplification of glucose-stimulated insulin secretion. *Physiological Reports*. **8**, e14420 (2020).

67. Q. Zhang, M. V. Chibalina, M. Bengtsson, L. N. Groschner, R. Ramracheya, N. J. G. Rorsman, V. Leiss, M. A. Nassar, A. Welling, F. M. Gribble, F. Reimann, F. Hofmann, J. N. Wood, F. M. Ashcroft, P. Rorsman, Na^{+} current properties in islet α- and β-cells reflect cell-specific Scn3a and Scn9a expression. *The Journal of Physiology*. **592**, 4677–4696 (2014).

68. W. Chen, I. Bergerot, J. F. Elliott, L. C. Harrison, N. Abiru, G. S. Eisenbarth, T. L. Delovitch, Evidence that a peptide spanning the B-C junction of proinsulin is an early Autoantigen epitope in the pathogenesis of type 1 diabetes. *J Immunol*. **167**, 4926–4935 (2001).

69. L. Haneskog, Preparation of Denatured Protein Samples from Inclusion Bodies. *Cold Spring Harb Protoc*. **2006**, 4265 (2006).

70. M. Umetsu, K. Tsumoto, M. Hara, K. Ashish, S. Goda, T. Adschiri, I. Kumagai, How additives influence the refolding of immunoglobulin-folded proteins in a stepwise dialysis system. Spectroscopic evidence for highly efficient refolding of a single-chain Fv fragment. *J Biol Chem*. **278**, 8979–8987 (2003).

71. R. Z. Cer, U. Mudunuri, R. Stephens, F. J. Lebeda, IC50-to-Ki: a web-based tool for converting IC_{50} to K_i values for inhibitors of enzyme activity and ligand binding. *Nucleic Acids Res*. **37**, W441–W445 (2009).

72. E. H. Ghazvini Zadeh, Z. Huang, J. Xia, D. Li, H. W. Davidson, W. Li, ZIGIR, a granule-specific Zn^{2+} indicator, reveals human islet α cell heterogeneity. *Cell Rep*. **32**, 107904 (2020).

73. Y. Zhou, B. Zhou, L. Pache, M. Chang, A. H. Khodabakhshi, O. Tanaseichuk, C. Benner, S. K. Chanda, Metascape provides a biologist-oriented resource for the analysis of systems-level datasets. *Nature Communications*. **10**, 1523 (2019).

74. Z. Gu, L. Gu, R. Eils, M. Schlesner, B. Brors, circlize implements and enhances circular visualization in R. *Bioinformatics*. **30**, 2811–2812 (2014).

75. A. Subramanian, P. Tamayo, V. K. Mootha, S. Mukherjee, B. L. Ebert, M. A. Gillette, A. Paulovich, S. L. Pomeroy, T. R. Golub, E. S. Lander, J. P. Mesirov, Gene set enrichment analysis: A knowledge-based approach for interpreting genome-wide expression profiles. *PNAS*. **102**, 15545–15550 (2005).

76. E. A. Vilas-Boas, L. Nalbach, E. Ampofo, C. F. Lucena, L. Naudet, F. Ortis, A. R. Carpinelli, B. Morgan, L. P. Roma, Transient NADPH oxidase 2-dependent H_2O_2 production drives early palmitate-induced lipotoxicity in pancreatic islets. *Free Radic Biol Med*. **162**, 1–13 (2021).

77. L. Nalbach, L. P. Roma, B. M. Schmitt, V. Becker, C. Körbel, S. Wrublewsky, M. Pack, T. Später, W. Metzger, M. M. Menger, F. S. Frueh, C. Götz, H. Lin, J. E. Manning Fox, P. E. MacDonald, M. D. Menger, M. W. Laschke, E. Ampofo, Improvement of islet transplantation by the fusion of islet cells with functional blood vessels. *EMBO Mol Med*. **13**, e12616 (2021).

78. S. M. Ireland, A. C. R. Martin, ZincBind-the database of zinc binding sites. *Database (Oxford)*. **2019**, baz006 (2019).

Acknowledgments:

The University of Alberta is situated on Treaty 6 territory, traditional lands of First Nations and Métis people. We thank the Human Organ Procurement and Exchange (HOPE) program and Trillium Gift of Life Network (TGLN) for their work in procuring human donor pancreas for research, and James Lyon (Alberta) for his efforts in human islet isolation. We especially thank the organ donors and their families for their kind gift in support of diabetes research.

Funding:

National Institutes of Health NIH R01 GM132610 (WL)

Canadian Institutes of Health Research Foundation Grant 148451 (PEM)

Sino-Canadian Studentship from Shantou University (HL)

Canada Research Chair in Cell Therapies for Diabetes (ARP)

Canada Research Chair in Islet Biology (PEM).

Author contributions:

Haopeng Lin[1, 2]†, Kunimasa Suzuki[1, 2]†, Nancy Smith[1, 2], Xi Li[3], Lisa Nalbach[4], Sonia Fuentes[3], Aliya F Spigelman[1, 2], Xiaoqing Dai[1, 2], Austin Bautista[1, 2], Mourad Ferdaoussi[6], Saloni Aggarwal[7], Andrew R Pepper[7], Leticia P Roma[5], Emmanuel Ampofo[4], Wen-hong Li[3], Patrick E MacDonald[1, 2] *

Conceptualization: HL, KS, ARP, EA, WL, PEM
Methodology: HL, KS, LN, LPR, ARP, EA, WL, PEM
Investigation: HL, KS, NS, XL, LN, SF, AFS, XD, AB, MF, SA, LPR
Visualization: HL, PEM
Supervision: ARP, LPR, EA, WL, PEM
Writing—original draft: HL, KS, PEM
Writing—review & editing: HL, KS, NS, XL, LN, SF, AFS, XD, AB, MF, SA, ARP, LPR, EA, WL, PEM

Competing interests:

Authors declare that they have no competing interests.

Data and materials availability:

All data are available in the main text or the supplementary materials.

Figure 1

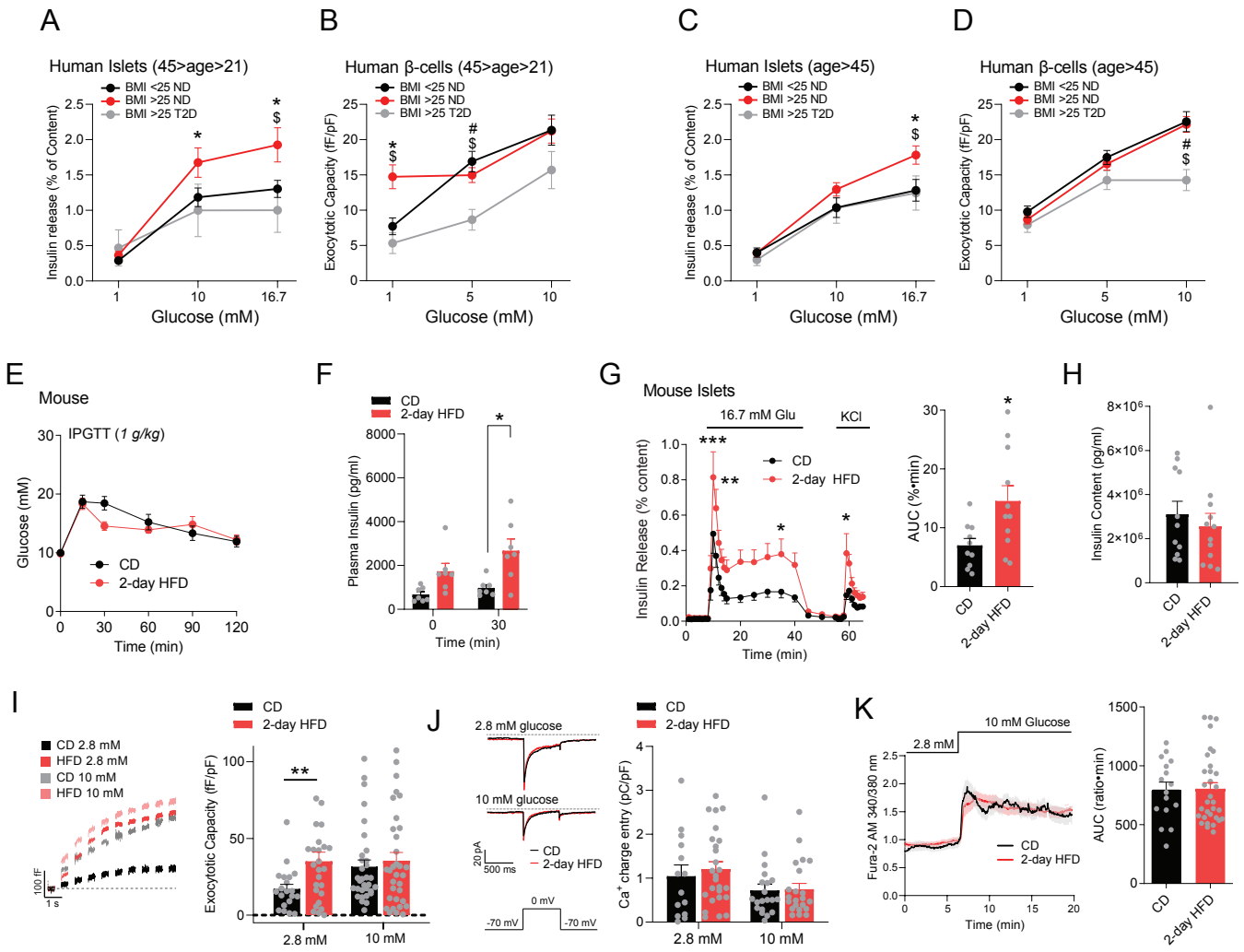

Figure 1. Islets from overweight human donors and 2-day HFD mice exhibited higher insulin secretion and exocytosis.

(A): Insulin secretion from islets of young adult (45>age>21) human donors. (n=27-47 donors without diabetes and 4-5 donors with T2D per condition). **(B):** Exocytotic response of β-cells from young (45>age>21) human donors. (n=11-33 donors without diabetes with 63-236 cells and 4-5 donors with T2D with 21-36 cells per condition). **(C):** Insulin secretion from islets of older (age>45) human donors. (n=40-111 donors without diabetes and 18-21 donors with T2D per condition). **(D):** Exocytotic response of β-cells from older (age>45) human donors. (n=30-73 donors without diabetes with 164-473 cells and 15-18 donors with T2D with 78-112 cells per condition). **(E):** IPGTT of C57 mice after CD and 2-day HFD (n=14 and 14 mice). **(F):** Plasma insulin level during IPGTT (n=7 and 8 mice). **(G):** Insulin secretion (n=10 and 11 mice). **(H):** Insulin contents (n=10 and 11 mice). **(I):** Representative traces (left), and average total responses, of β-cell exocytosis elicited by a series of 500 ms membrane depolarizations from -70 mV to 0 mV at 2.8- and 10-mM glucose (n=3 pairs of mice, n=21-33 cells). **(J):** Representative traces, and average voltage-dependent Ca^{2+} currents, of β-cell elicited by a single 500 ms membrane depolarization from -70 mV to 0 mV at 2.8- and 10-mM glucose (n=15-26 cells). **(K):** Single cell calcium response (n=16, 34 cells from 5 and 4 mice). Data are mean ± SEM and were compared with student t-test, one-way or two-way ANOVA followed by Bonferroni post-test. *p < 0.05, **p < 0.01 unless in A-D, *p < 0.05 (BMI>25 ND vs BMI<25 ND), $p < 0.05 (BMI>25 ND vs BMI>25 T2D), #p < 0.01 (BMI<25 ND vs BMI>25 T2D).

Figure 2

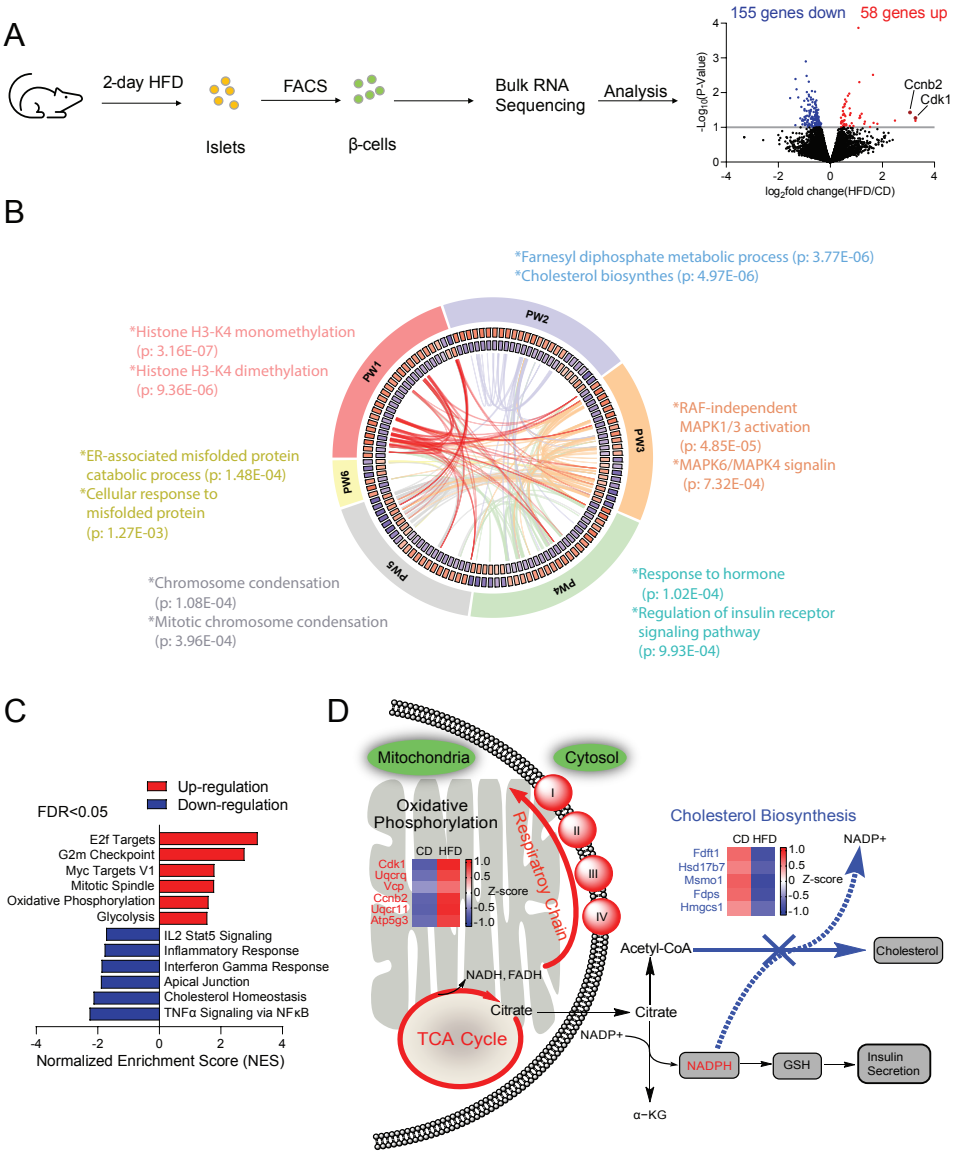

Figure 2. RNA sequencing suggests remodeling of metabolic pathways following 2-day HFD

(A): β-cells from CD and 2-day HFD were isolated through fluorescence activated cell sorting (FACS) for mRNA sequencing. 213 genes were identified differentially expressed (DE) genes after 2-day HFD (n=213 genes, N=4, 3 mice). **(B):** All DE genes were submitted to Metascape for functional enrichment analysis. Expression of DE genes on CD and HFD were normalized to z-scores by gene and colorized in circos heat map. Enrichment and cluster analysis were performed on Metascape and six most enriched pathway (PW) illustrated as circos plot. All DE genes were submitted to STRING database for protein-protein interaction. The related protein interactions for DE genes enriched in the six PW were highlighted as links in the circos plot. **(C):** Gene set enrichment analysis (GSEA) showed significant up- and down-regulated enriched pathway after HFD with false discovery rate (FDR) less than 0.05. All nominal p-value were less than 0.01. Normalized enrichment score (NES) reflects the degree to which a gene set is overrepresented in a ranked list of genes. **(D):** Illustration of transcriptomic changes related to metabolism after 2-day HFD.

Figure 3

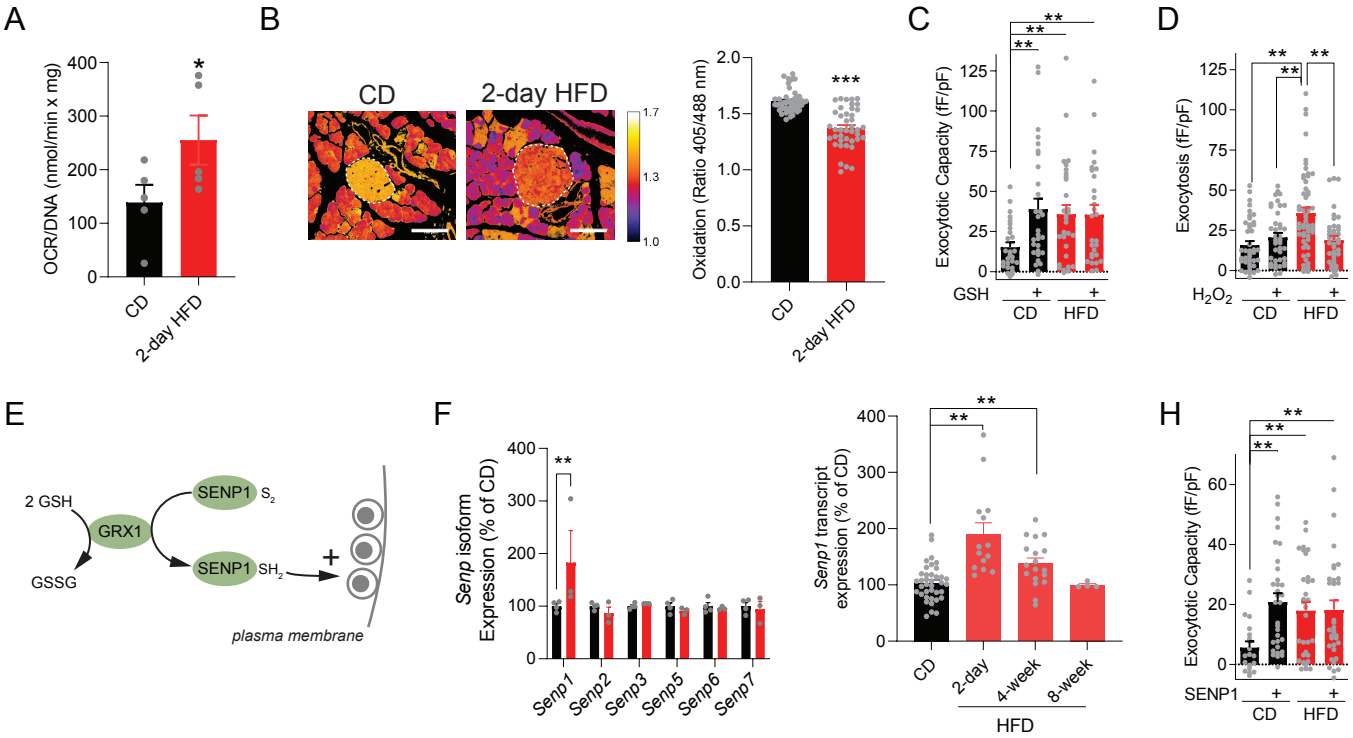

Figure 3. Cytosolic redox signaling via SENP1 contributes to enhanced exocytosis during 2-day HFD

(A): Oxygen consumption rate at 2.8 mM glucose (n=4, 5 mice). **(B):** Representative image of pancreatic islets carrying cyto-roGFP2-Orp1 sensor (left). Scale bar = 100 µm. Redox ratio of individual islets (n= 65, 41 islets from 6 pairs of mice). **(C, D):** Exocytosis with infusion of (C) 10 µM GSH or (D) 200 µM H2O2 at 2.8 mM glucose after 2-day HFD. (C - n=26-56 cells from 4, 4 mice, D - n= 39-56 cells from 7, 7 mice). **(E):** Illustration of redox-controlled insulin secretion. Reduced glutathione (GSH) activates glutaredoxin-1 (GRX1), followed by reducing power transfer from GRX1 to SENP1 and activation of SENP1, finally enhancing insulin exocytosis. **(F):** *Senp* isoform expression from RNA sequencing of purified β-cells from chow or HFD fed mice (n=4, 3 mice). **(G):** *Senp1* mRNA expression after HFD assessed by quantitative PCR (n=2-9 mice). **(H):** Exocytosis with infusion of 4 µg/mL catalytic SENP1 (cSENP1). (n=21-33 cells from 4, 4 mice per group) at 2.8 mM glucose. Data are mean ± SEM and were compared with student t-test, one-way ANOVA followed by Bonferroni post-test. *p < 0.05, **p < 0.01, ***p < 0.001.

Figure 4

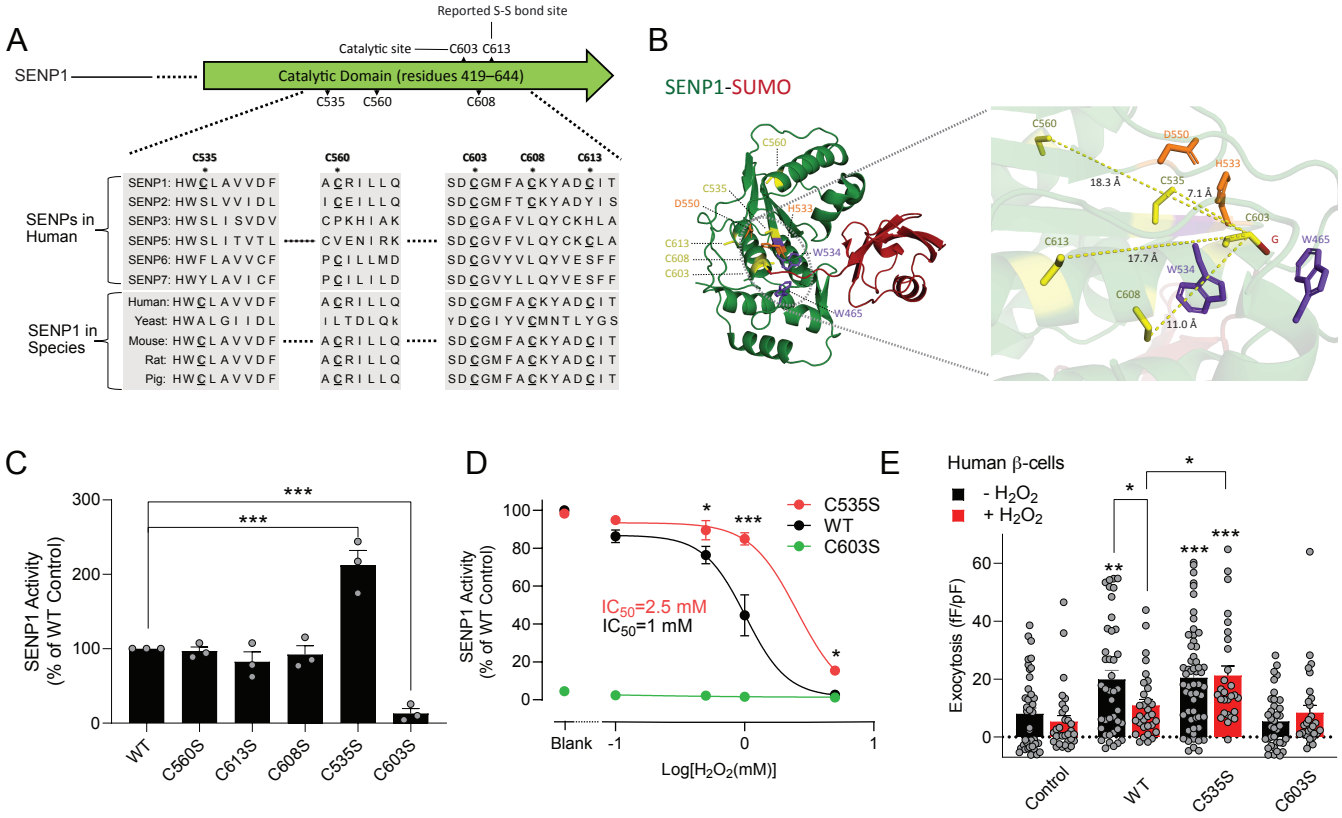

Figure 4. SENP1 catalytic activity is regulated by redox state through C535

(A): Multiple amino acid comparison among different isoforms of SENP across species. **(B):** Structure representation of SENP1-SUMO complex (ID: 2IYD, SENP1: green. SUMO: red) from PDB database. Potential redox-sensing cysteines (C535, C560, C603, C608, C613, yellow: C603 is a catalytic site), another two catalytic triad (D550, H533, orange), and catalytic "floor" (W534, purple blue) and "lid" (W465, purple blue) were labeled. On the right panel, the catalytic region along with potential cysteines were outlined and zoomed in. Dashed lines indicated the measured distance (Å) between thiol group from catalytic (C603, yellow) to the ones from other potential cysteines (C535, C560, C603, C608, C613, yellow). **(C):** Measurement of SENP1 activity after cysteine-to-serine substitution (n=3). **(D):** Dose-response curve of SENP1 inhibition by H_2O_2 (n=3). **(E):** 4 µg/mL glutathione-S-transferase (GST) peptide (control), SENP1 WT, C535S and C603 were infused into human β-cells with/without 200 µM H_2O_2 to assess their effects on exocytosis at 5 mM glucose (n=28-46 cells per group from 7 human donors). Data are mean ± SEM and were compared with student t-test, one-way ANOVA or two-way ANOVA followed by Bonferroni post-test. *p < 0.05, **p < 0.01, ***p < 0.001. In panel D, * indicates comparison between SENP1 WT and C535S.

Figure 5

A

SENP1 WT

Predicted Zinc-bind Site	Probability
Cys603, Cys535, His533	1
Asp550, His533	1
Asp468, His529	1
Asp517, His491	1
Asp529, His533, His539	1
Glu430, His640	0.96

SENP1 C535S mutant

Predicted Zinc-bind Site	Probability
Asp550, His533	1
Asp468, His529	1
Asp517, His491	1
Glu430, His640	0.96

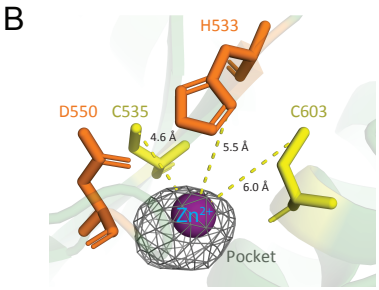

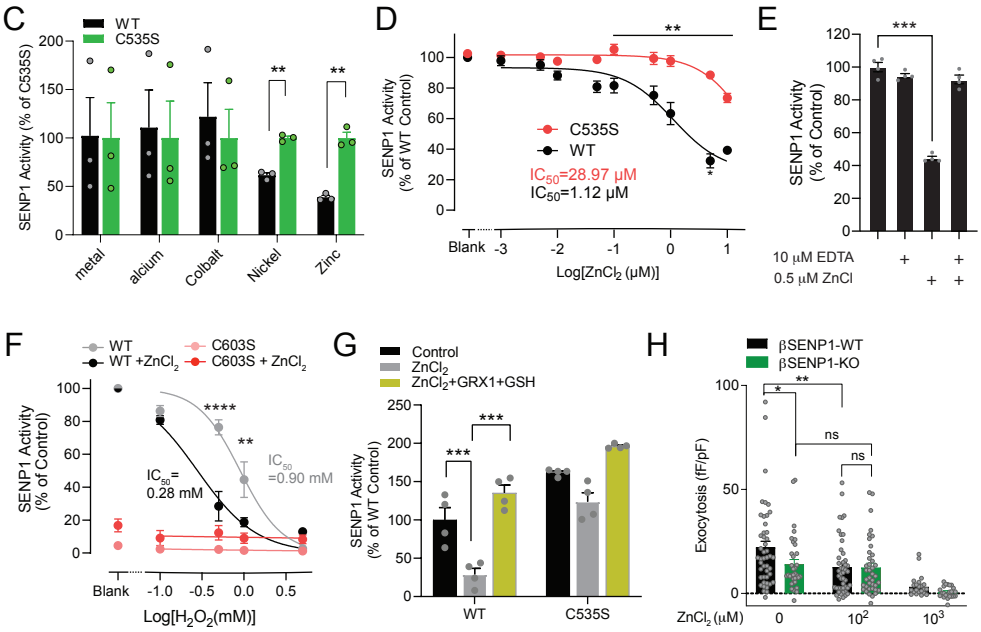

Figure 5. Binding of Zn^{2+} to C535 regulated SENP1 redox sensitivity

(A): Prediction of Zn^{2+}-binding site in SENP1 WT (ID: 2IYC) and C535S mutant derived from SENP1 WT (ID: 2IYC) using Pymol mutagenesis. **(B):** Illustration of zinc binding to C535, H533 and C603. **(C):** Effect of different metal ions on SENP1 activity. Data are normalized to WT. C535S mutant activity was more stable and resistant to oxidation (n=3). **(D):** Dose-response curve of SENP1 inhibition by $ZnCl_2$ (n=3). **(E):** SENP1 inhibition by $ZnCl_2$ could be removed with chelating reagent EDTA. **(F):** Dose-response curve of SENP1 mutants prepared with or without $ZnCl_2$ under inhibition with H_2O_2 (n=3-6). **(G):** Wild-type SENP1 and mutants were reduced with 5 mM reduced glutathione and 10 μg/ml glutaredoxin-1 (GSH+GRX1) after inhibition with 1 μM $ZnCl_2$ (n=4). **(H):** Effect of Zn^{2+} on exocytosis from βSENP1-KO mouse β-cells at 5 mM glucose (n= 23-46 cells from 6 pairs of mice). Data are mean ± SEM and were compared with one-way ANOVA or two-way ANOVA followed by Bonferroni post-test. *p < 0.05, **p < 0.01, ***p < 0.001.

Figure 6

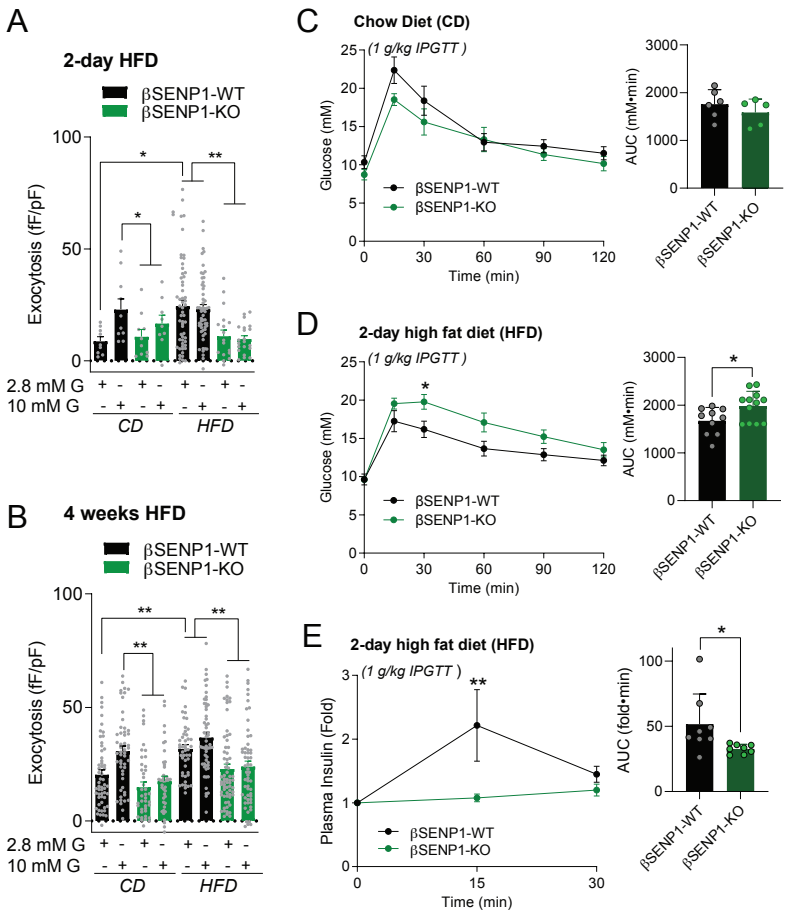

Figure 6. βSENP1-KO mice rapidly developed impaired IP glucose tolerance following 2-day HFD

(A-B): Exocytotic response of single β-cells from βSENP1-WT and βSENP1-KO mice after 2-day and 4-week HFD (A - n=18-56 cells, B - n=30-65 cells). **(C-D):** IP glucose tolerance test (IPGTT) of male βSENP1-WT and βSENP1-KO mice fed with CD (C - n=6, 5) and 2-HFD (D - n= 10, 12). **(E):** Plasma insulin response during the IPGTT after the 2-day HFD (n=8, 8). Data are mean ± SEM and were compared with student t-test or two-way ANOVA followed by Bonferroni post-test. *$p < 0.05$, **$p < 0.01$.